i-Motif-Driven Au Nanomachines in Programmed siRNA Delivery for Gene-Silencing and Photothermal Ablation

Sejin Son,[†,‡,§] Jutaek Nam,[‡,§] Jinhwan Kim,[†,‡] Sungjee Kim,[‡] and Won Jong Kim[†,‡,*]

[†]Center for Self-Assembly and Complexity, Institute for Basic Science (IBS), Pohang, 790-784, Korea, and [‡]Department of Chemistry, Pohang University of Science and Technology (POSTECH), Pohang, 790-784, Korea. [§]S. Son and J. Nam contributed equally to this work.

ABSTRACT The present work illustrates unique design, construction and operation of an i-motif-based DNA nanomachine templated on gold nanoparticles (AuNPs), which utilizes pH-responsive dynamic motion of i-motif DNA strands and aggregational behavior of AuNPs to elicit programmed delivery of therapeutic siRNA. The pH-sensitive nucleic acids immobilized on the AuNPs consisted of three functional segments, *i.e.*, an i-motif DNA, an overhanging linker DNA and a therapeutic siRNA. At neutral pH, the i-motif DNA is hybridized with the overhanging linker DNA segment of the therapeutic siRNA. However, in endosomal acidic pH, the i-motif DNA forms interstrand tetraplex, which could induce cluster formation of AuNPs resulting in endosomal escape of AuNP clusters, and produce a high gene silencing efficiency by releasing siRNA in the cytosol. Furthermore, the cluster formation of AuNPs accelerated photothermal ablation of cells when irradiated with laser. Precise and synchronized biomechanical motion in subcellular microenvironment is realized through judicious integration of pH-responsive behavior of the i-motif DNA and AuNPs, and meticulous designing of DNA.

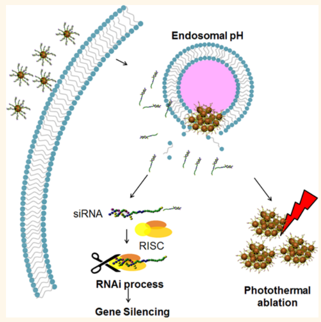

KEYWORDS: photothermal effect · pH-responsive · endosome disruption · i-motif · siRNA delivery

Living organisms evolve numerous molecular machines to generate various biological motions including intracellular material transport to accomplish diverse cellular tasks.[1,2] Recent advances in nanotechnology have spawned a plethora of research efforts to mimic and regulate various biological functions through the generation of artificial nanomachines.[3,4] However, the deployment of such artificial nanomachines in a living body, especially for therapeutic purposes necessitates robust dynamic motion and highly exquisite multifunctional attributes. In particular, nanomachines driven by external stimuli such as light, temperature, magnetic field and ultrasound or responsive to intracellular stimuli such as enzymes, pH and reductive environment could deliver payloads or generate heat by modulating its morphology or aggregation behavior after cellular uptake.[5−7]

To this end synthetic DNA-based nanomachines owing to their extreme sequence specificity, favorable physiochemical properties, and programmable supramolecular self-assembly emerge as an enticing prospect for artificial nanomachines,[8,9] and are being exploited to yield molecular switches, motors, and sensors[10−12] by generating forces and motion through stimuli-responsive conformational metamorphosis. Numerous efforts have been made to exploit DNA nanomachine in delivering payloads but are mostly restricted to small molecules and could be hardly extended toward nucleic acid delivery under biological environment due to their rudimentary design and structural inadequency.[13−16] Recently, we reported a functionalized reduced graphene oxide (PEG-BPEI-rGO) as a nanotemplate for photothermally triggered cytosolic drug and gene delivery by inducing endosomal disruption.[17,18] We assume that an elaborately designed DNA nanomachine can also be escaped from endosome, which is a very critical process during payload delivery.

Here, we describe a sophisticated effort to engineer a DNA-based hybrid nanomachine templated on gold nanoparticles (AuNPs) (denoted as DNA-Au nanomachine) through a rational design, and a successful application of a dynamic therapeutic DNA-Au nanomachine operating within living cells. This nanomachine exploits the design

* Address correspondence to wjkim@postech.ac.kr.

Received for review December 15, 2013 and accepted May 28, 2014.

Published online May 28, 2014
10.1021/nn5022567

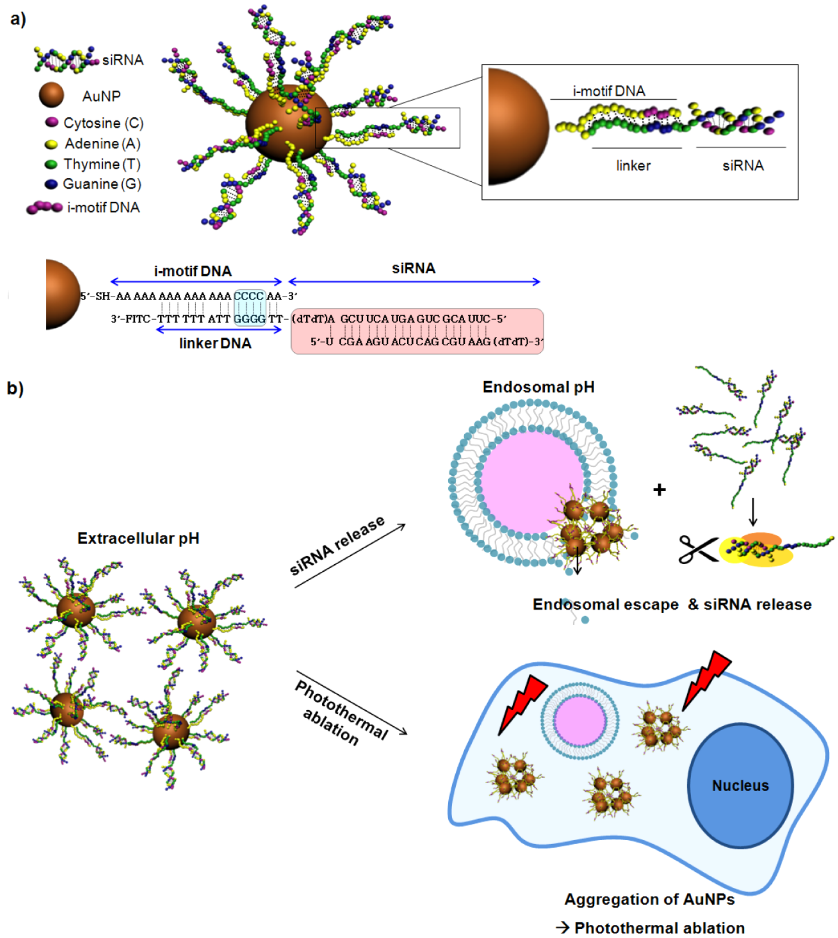

Figure 1. siRNA-loaded pH-responsive DNA nanomachine. (a) Schematic description of DNA nanomachine. The i-motif DNA is covalently conjugated to AuNP, and siRNA was linked to AuNP *via* hybridization of i-motif DNA with linker DNA. (b) pH-responsive aggregation of siRNA-i-motif-AuNP for endosomal escape, siRNA release, and photothermal ablation.

principles of an i-motif DNA nanomachine that transduces pH gradients into crucial conformational changes in nucleic acids conjugated on a AuNP surface.[19,20] The ability of i-motif sequence to form DNA i-tetraplex consisting of two parallel-stranded C:C$^+$ hemiprotonated base-paired duplexes intercalated in an antiparallel orientation[21,22] could be harnessed to trigger gene silencing through the programmed release of therapeutic siRNA hybridized to i-motif DNA *via* linker DNA (Figure 1a). Moreover, the DNA i-tetraplex formation between i-motif DNA sequences of AuNPs concomitantly induces the reversible formation of Au clusters (AuCs), eliciting coupled surface plasmons and strong absorption at far-red and near-infrared (NIR) wavelengths with efficient heat conversion. This locally induced heat generation leads to photothermal ablation (Figure 1b). Aiming at constructing a sophisticated and advanced nucleic acid delivery system, our work judiciously utilizes highly diverse and advantageous biophysical and optical features of nucleic acids and AuNPs, respectively. Our approach ingeniously integrates these desirable features of nucleic acids and AuNP in an intriguing fashion to develop a pH-responsive dynamic nanomachine. In addition, the design of the DNA-Au nanomachine provides a protective nucleic acid layer imparting colloidal stability to bare AuNPs, which is perceived to be critical physicochemical property for systemic delivery. In this study, we examined the design principle of DNA-Au nanomachine, pH-triggered aggregation behavior and gene silencing efficiency by siRNA delivery. We also carefully investigated the synergistic effect of DNA-Au nanomachine for gene silencing and photothermal cell ablation.

RESULTS AND DISCUSSION

Design of Nucleic Acid-AuNP Nanomachine. The pH-sensitive nucleic acids immobilized on AuNP consisted of three functional segments, *i.e.*, an i-motif DNA, an overhanging linker DNA and a therapeutic siRNA (Figure 1a). 5′-Thiolated i-motif DNA sequence constitutes the motor segment of nanomachine and contains cytosine (C) rich region, which is transformed into a unique tetrameric i-motif structure under acidic condition. At neutral pH, the 5′-thiolated i-motif DNA is hybridized with the overhanging linker DNA segment of the therapeutic siRNA. Thus, the overhanging linker DNA acts as the fusion template for pH-sensitive

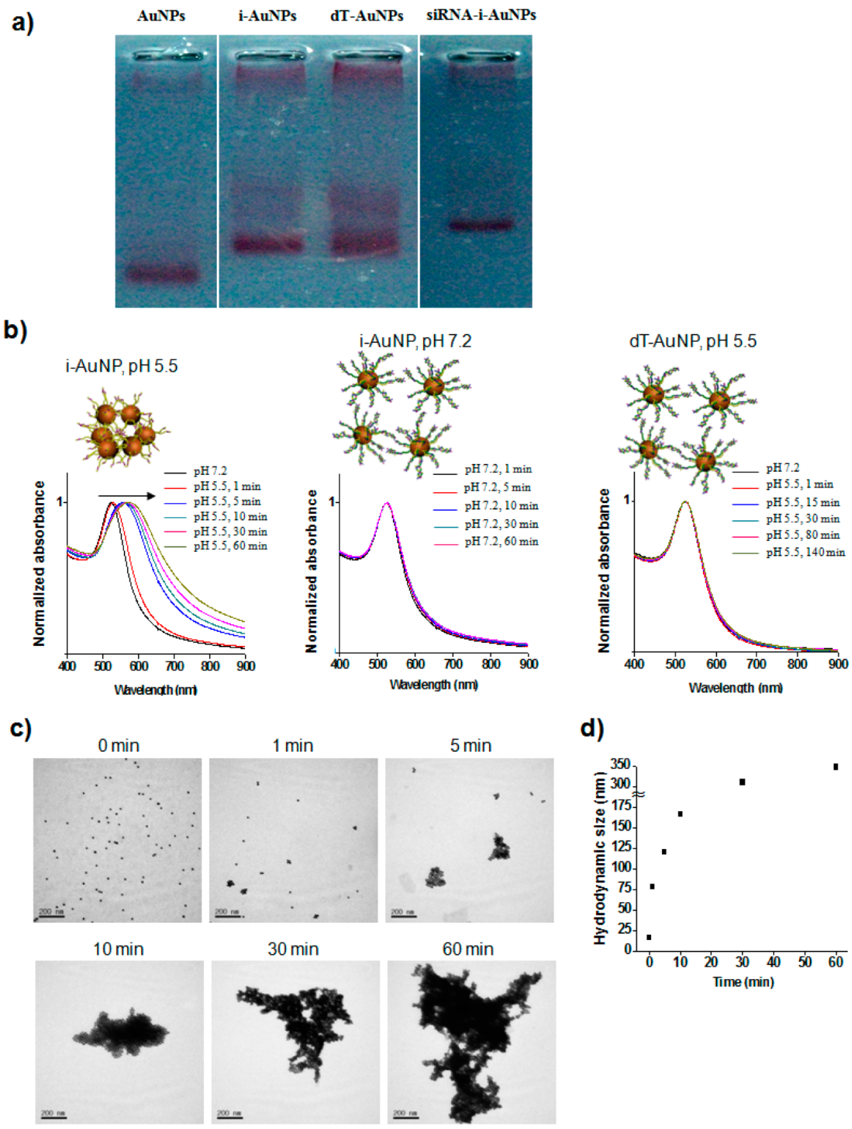

Figure 2. pH-responsive aggregation of the DNA nanomachine. (a) Confirmation of DNA nanomachine by gel electrophoresis. (b) UV−vis spectroscopic study of DNA-modified AuNP aggregation at pH 5.5 and pH 7.2. Aggregation of i-motif-AuNPs is monitored under acidic (left) and neutral (middle) pH. pH-insensitive deoxythymidine-modified AuNP (dT-AuNP) was used as a control (right). (c) TEM images of i-motif-AuNPs are obtained at pH 5.5 with different elapsed times of 0, 1, 5, 10, 30, and 60 min. (d) The hydrodynamic size of i-motif-AuNPs at pH 5.5 are monitored by dynamic light scattering (DLS).

i-motif-modified AuNP and the therapeutic siRNA. The i-motif/linker DNA hybridized motor segment operates as a tunable switch to release siRNA through the pH-triggered conformational change in DNA at body temperature. Therefore, the centerpiece of our design is embodied in achieving the crucial control over the conformational changes and thus triggering siRNA release through the fine-tuning of the length and sequence of linker DNA. The difference in thermal stability of nucleic acids and external pH induces sequence-dependent separation and conformational change of double-stranded nucleic acids, which ensures the necessary dynamic and controlled association/dissociation of pretailored nucleic acid structures. Lastly, the therapeutic segment composed of therapeutic siRNA, to treat or detect target disease, can also be replaced by other nucleotide-based therapeutics such as antisense DNA and mRNA as per the therapeutic needs.

Preparation and pH-Responsive Behavior of DNA-Au Nanomachine. Citrate-stabilized AuNPs (∼15 nm) (Figure S1, Supporting Information) were prepared and successfully functionalized with the thiolated i-motif DNA or duplexes of i-motif DNA/siRNA-linker chimeric strands through a salt aging process to yield densely DNA-covered AuNPs having hydrodynamic sizes in the following order: siRNA-loaded i-motif-AuNPs (siRNA-i-AuNP) > i-motif-modified AuNP (i-AuNP) > AuNPs modified with short C4 (CCCC) DNA (Figure 2a and Figure S2, Supporting Information). Prior to the study of pH-dependent aggregation behavior of the nanomachine, buffer composition of this system was optimized. Parameters such as crowding effect of the surface-immobilized DNA strands and electrostatic charge repulsion between negatively charged DNAs should be considered as critical factors that have highly affected the behavior of DNA-mediated AuC formation. To offset electrostatic repulsion among DNA strands and thus stabilize the DNA structure, 10 mM $MgCl_2$ was added to the DNA-AuNP solution (Figure S3, Supporting Information). Then, pH-dependent reversible aggregation behavior of the i-AuNPs were established by UV–vis spectroscopic studies, which showed a resonance shift in absorption from 525 to 615 nm (Figure 2b) with decreasing pH from 7.2 to 5.5, and the result was further substantiated by transmission electron microscopy (TEM) images (Figure 2c) and hydrodynamic size measurement (Figure 2d). As shown in Figure 2b,c,d, in acidic pH 5, i-motif-AuNP formed large size aggregates, but no aggregation behavior of AuNPs was observed in neutral pH or a pH-insensitive deoxythymidine modified AuNPs (dT-AuNPs).

TABLE 1. Sequence of Linker DNA, Melting Temperature (T_m[a]), and pH-Responsiveness of AuNPs

name	sequence (5′→3′)	T_m[a]/°C	pH-responsiveness
i-motif	AA AAA AAA AAA AAA CCC CAA		
L20-T14	TTG GGG TTT TTT TTT TTT TT	58.4 (41.5)[b]	n.d.
L15-T9	TTG GGG TTT TTT TTT	52.3 (21.4)[b]	n.d.
L15-T8A1	TTG GGG TTA TTT TTT	44.1 (20.4)[b]	yes
polydT	TTT TTT TTT TTT TTT TTT TT		
L20-A20	AAA AAA AAA AAA AAA AAA AA	52.6	n.d.
L15-A15	AAA AAA AAA AAA AAA	43.9	n.d.
L15-A14T1	AAA AAA AAT AAA AAA	33.7	n.d.

[a] T_m was calculated by IDT's T_m calculator (OligoAnalyzer 3.0 in SciTools at www.idtdna.com). [b] Calculated with oligo-dT except TTGGGG region. n.d. stands for not detected.

The contrasting pH-dependent aggregation and spectral behavior of i-AuNPs and control dT-AuNPs (Figure 2 and Figure S4, Supporting Information) exemplifies the indispensability of the sequence specificity of i-AuNPs in enforcing pH-responsive aggregation and the related spectral shift. Interestingly, formation of parallel duplexes by polydeoxyadenosine (polydA) at acidic pH[23] prompted us to select polydA as a spacer between i-motifs and AuNPs, anticipating its synergistic effect in triggering pH-dependent AuC formation (Figure S5, Supporting Information). Fueled by the pH-induced conformational changes within DNA, the i-motif-based nanomachine, consisting of i-AuNPs and siRNA linked together by linker DNA, generated

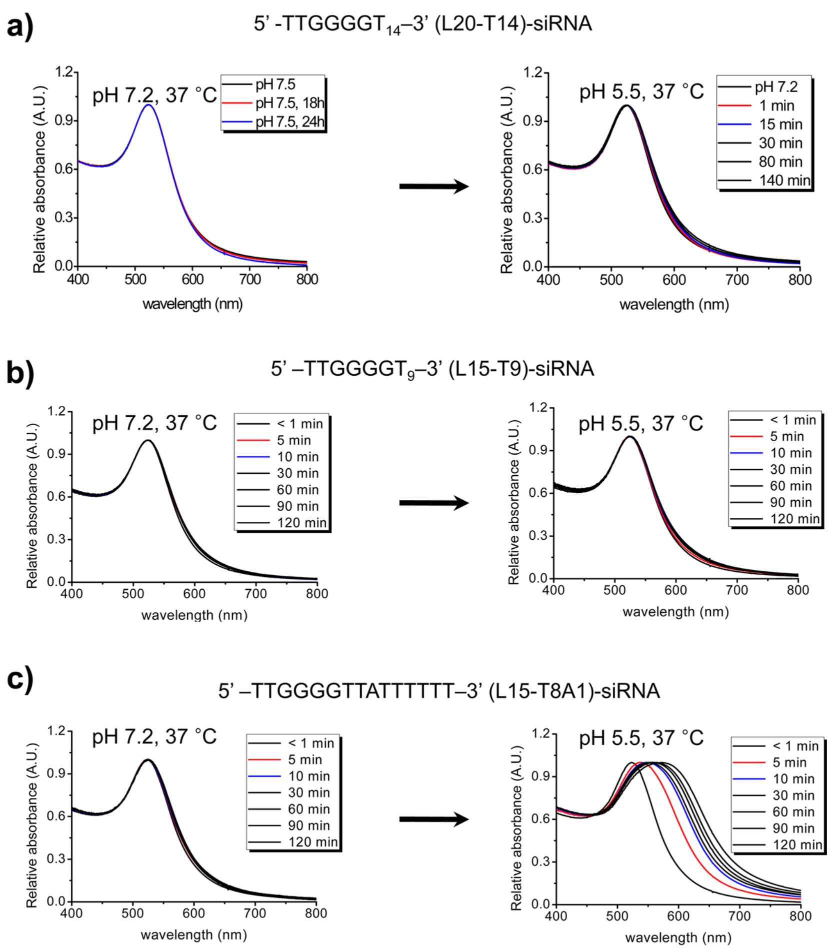

Figure 3. pH-dependent aggregation of i-AuNP/siRNA-linker. (a) L20-T14-siRNA/i-AuNP. (b) L15-T9-siRNA/i-AuNP. (c) L15-T8A1-siRNA/i-AuNP.

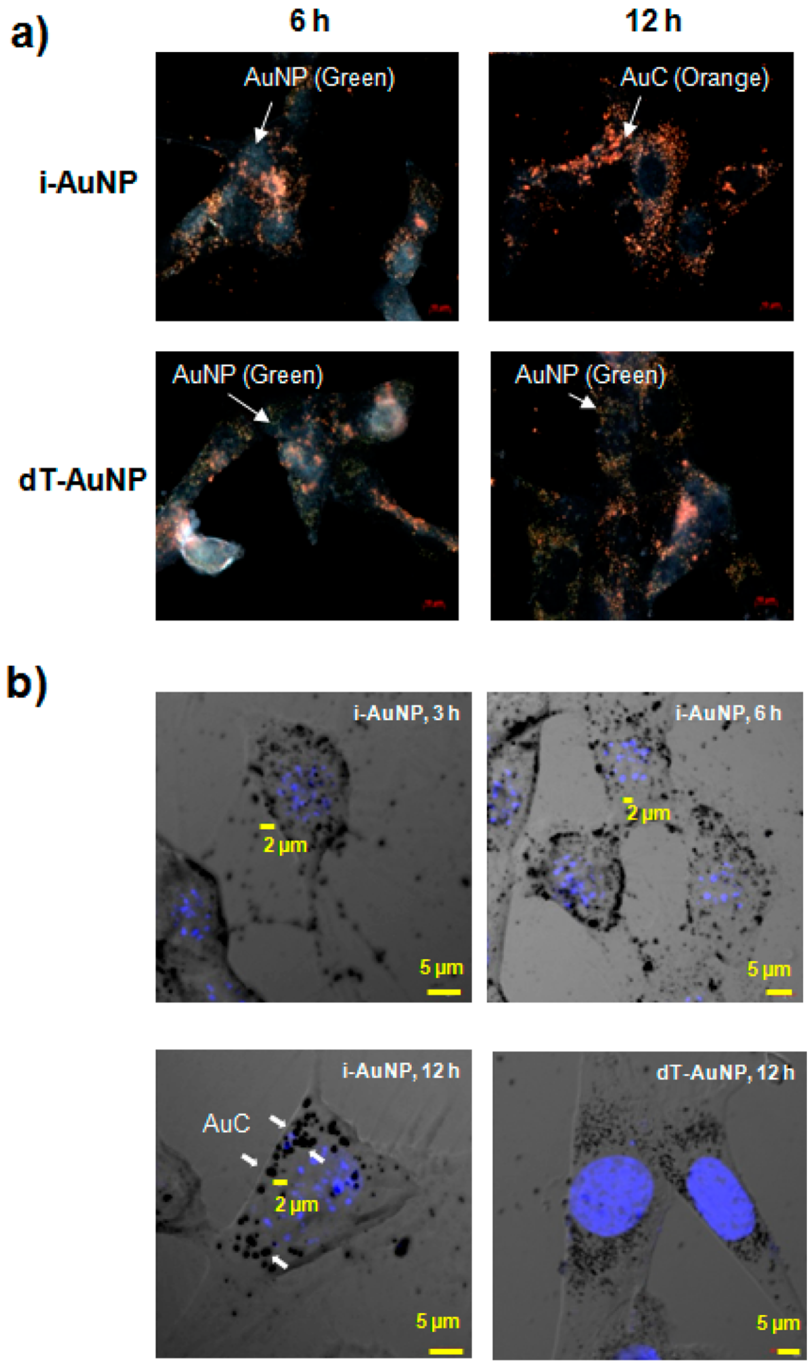

Figure 4. Monitoring of AuC formation. (a) Dark-field microscope images of NIH3T3 cells treated with 20 nM of i-AuNPs and dT-AuNPs. (b) DIC images of intracellular AuC formed by i-AuNPs and dT-AuNPs with various incubation times.

dynamic motions as evidenced by AuNP aggregation and concomitant siRNA-release at endosomal pH.

Systematic Development of Linker DNA. To synchronize the release of therapeutic siRNA with the motion of the nanomachine, the hybridization between the pH-sensitive i-motif DNA strand and the complementary overhanging linker DNA carrying the therapeutic siRNA must be tuned appropriately (Figure 1a). The hybridized chimeric duplex (i-motif/siRNA-linker) should remain stable at physiological pH and body temperature (pH 7.2 at 37 °C) until cellular internalization, but upon internalization must ensure dehybridization at endosomal pH at body temperature (pH 5.5 at 37 °C) to elicit siRNA detachment from the surface of i-motif-linked AuNPs, and trigger AuNP aggregation and siRNA release (Figure 1b). Since the half-protonated C-rich region of the i-motif accelerates destabilization of the chimeric duplex through i-motif formation, it is expected that the destabilization not only facilitates the release of therapeutic siRNA but also induces AuNP aggregation. If i-motif formation fails to exert sufficient driving force to trigger complete dehybridization of

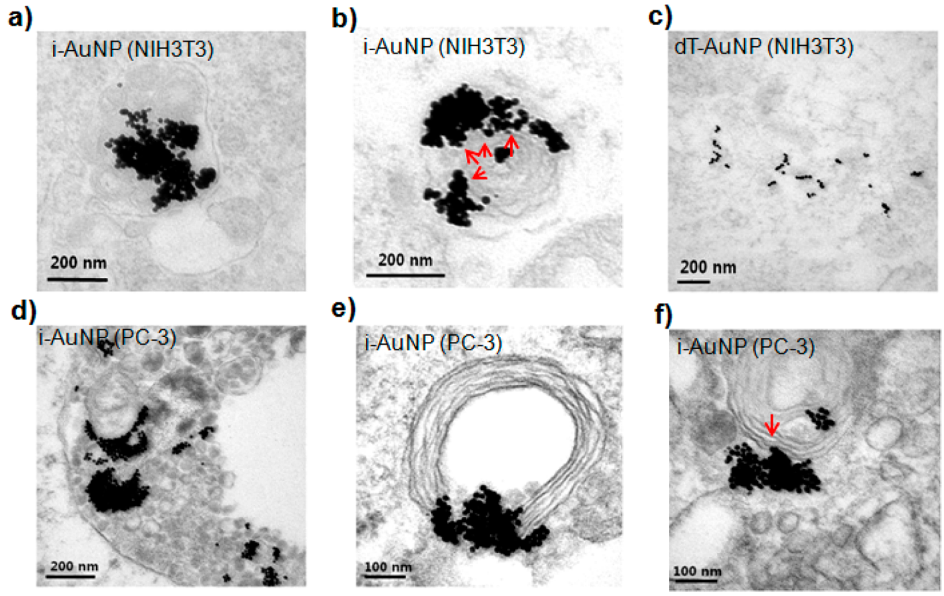

Figure 5. TEM images of subcellular localized AuNPs obtained in NIH3T3 cells (a–c) and in PC-3 cells (d–f). Cells were treated with i-AuNPs (a, b, d, e and f) and dT-AuNPs (c).

the chimeric duplex, thermodynamic stability should be regulated by manipulating the length and number of mismatched bases of linker DNA. Using a systematic approach, we designed therapeutic siRNA having a 20-base linker sequence (L20-T14 in Table 1 and Figure 3a) as an overhanging region that was preset to be hybridized with the i-motif DNA strand of AuNPs. However, no UV–vis spectral and colorimetric changes were observed at the lower pH of 5.5 at 37 °C, even after 1 day, which indicated a strong hybridization between the linker DNA and its complementary i-motif DNA strand (Figure 3a). Theoretical calculation of the melting temperature (T_m) of DNA hybridization using T_m calculator revealed the T_m of the 20-base linker as 58.4 °C, in which the T_m of the oligo-dT region excluding TTGGGG was expected to be 41.5 °C. This result implied that even after destabilization of the i-motif region at a lower pH, the T_m of the 20-base linker still remained too high to be dissociated. To reduce the thermodynamic stability of the linker, we chose a 15-base DNA length (L15-T9 in Table 1) with a T_m of 52.3 °C as a spacer. The theoretical calculation predicted the T_m of the oligo-dT sequence, excluding the i-motif TTGGGG region, as 21.4 °C, which lies below body temperature and anticipated to trigger dissociation of the oligo-dT region once the i-motif sequence formed its i-tetraplex at low pH. However, contrary to our expectations, no aggregation of AuNPs was observed, presumably due to enhanced stability conferred by the multivalent effect of the DNA linked to the AuNP template (Figure 3b).[24] On the basis of this assumption, we inserted a one-base mismatch into the 15-base linker (L15-T8A1 in Table 1) to reduce duplex stability, which indeed accelerated the duplex dissociation rate as evidenced by a color change from red to purple accompanied by a red shift exhibiting i-motif-mediated AuC formation (Figure 3c). Hence, a careful design of the linker DNA furnished an intelligent nanomachine actuated to function in response to subtle pH changes at body temperature. Noticeably, for dT-AuNP, no linker showed pH-responsive AuC formation, rendering them incompatible with this device (Figure S4a and S6, Supporting Information).

Study of Cellular Uptake and Endosomal Escape of DNA-Au Nanomachine. Observed efficient cellular uptake through endocytosis[25–27] (Figure S7, Supporting Information) provided an ideal platform for successful intracellular pH-triggered action of the nanomachine, even without the aid of transfection agents. To visualize *in vitro* pH-triggered AuC formation and siRNA release as evidence of proper functioning of the nanomachine, we utilized the optical contrast arising from the coupled plasmon-induced distance-dependent scattering properties of AuNPs and investigated the intracellular performance of the nanomachine triggered by pH drop along with the AuC formation *via* i-motif formation. The size-dependent light scattering property of AuNPs[28,29] offers direct evidence of macroscopic AuC formation within living cells upon exposure to low endosomal pH. This was evidenced as distinct change in scattered light color from green-yellow to orange-red light (Figure 4a). Mapping of the i-AuNPs and control dT-AuNPs within NIH3T3 cells using dark-field optical microscopy clearly showed the efficient cellular internalization of the nanomachine over time. The i-AuNPs predominantly formed AuCs (orange) with sizes of hundreds of nanometers, whereas dT-AuNPs lacking the i-motif sequence remained discernible as discrete NPs (green) during the cell endocytic process (Figure 4a). Upon exposure to the pH drop in cell endosomes, i-AuNPs alone yielded

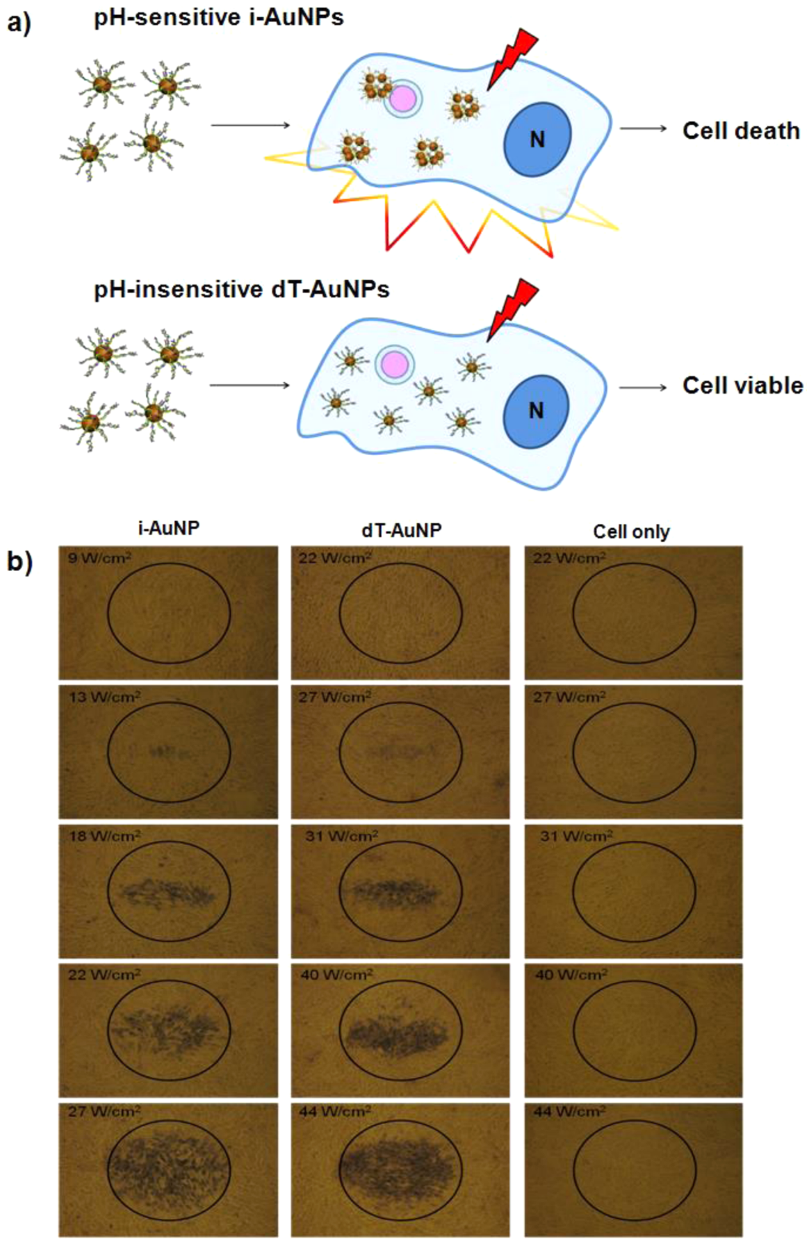

Figure 6. Photothermal ablation by DNA nanomachine. (a) Schematic description of DNA nanomachine-mediated photothermal ablation. (b) Cell death profile. NIH3T3 cells were incubated with i-AuNPs (left), dT-AuNPs (middle) and without AuNPs (right). Laser fluence rates are 9, 13, 18, 22, 27, 31, 40, and 44 W/cm^2 from top to bottom row. Circles denote the position of the laser spot.

intracellular AuC formation and interparticle distance-dependent optical behavior evidenced by surface plasmons. This aggregation could also effectively prevent the exocytosis of internalized AuNPs due to this increased size and thereby induced greater cellular accumulation of AuNP aggregates augmenting the surface plasmon resonance and photothermal therapy at the targeted site.[30,31]

Different interference contrast (DIC) images of the internalized i-AuNPs (Figure 4b) revealed more precise and prominent visualization of interspersed AuC as black spots within the cytosol. The gradual growth of AuC sizes up to several micrometers ($\sim\mu$m, refer to scale bar) after 12 h by coalescence of evenly distributed smaller AuCs within the cytoplasmic region was clearly evident. As expected, dT-AuNPs, corroborating dark-field microscopic analysis (Figure 4a), appeared as blurred and smaller black spots without discernible intracellular accumulation and cluster formation (Figure 4b).

TEM-assisted visualization of AuCs at the submicrometer level revealed interesting subcellular details such as the precise location of AuC formation during the endocytosis and endosomal escape, which remained inconspicuous during confocal microscopic studies. Most i-AuNPs were detected as clusters

(100–300 nm) exclusively inside vesicles in NIH3T3 and PC-3 cell lines (Figure 5a,b,d,e,f) even at high magnification, implying consistent aggregation of i-AuNPs at endosomal pH. In contrast, dT-AuNPs in these cell lines were located discretely throughout the cytosol or confined within the vesicles in small clusters (Figure 5c). The AuCs also displayed a highly interesting and intriguing feature of endosomal escape in real time. Microscopic images vividly captured precise moments with immaculate clarity when AuCs perforated the endosomal membrane during endosomal escape (Figure 5e). Other images confirmed the presence of relatively large AuCs (>100 nm) protruding through the ruptured vesicle membranes (red arrow in Figure 5b,f). Importantly, the presumed AuCs-mediated endosomal disruption during i-motif formation facilitated the release of endosomal contents (therapeutic siRNA) to the cytosol enabling endosomal rupture unaided by any cationic moiety or cell-penetrating peptide.[32,33] Successful internalization, intracellular AuC formation, and viable endosomal release advocated the therapeutic potential of these fabricated hybrid nanoconstructs (Figure 5 and Figure S7 and S8, Supporting Information).

DNA-Au Nanomachine-Mediated Photothermal Ablation in Cells. As designed, a pH trigger turns on i-motif formation, which in turn sets off a dynamic action within the endosome leading to siRNA release and AuC formation, deemed crucial to generate heat. Nanomachine-mediated photothermal effects on NIH3T3 cells were studied using CW diode laser irradiation at 660 nm as described in Figure 6a. Only aggregated variants of AuNPs should absorb this wavelength (Figure 2b). Normally, the threshold laser power to impose cell death is inversely proportional to the extent of AuNP aggregation; higher aggregation facilitates absorption of laser light at lower laser fluence. The observed threshold laser power required to inflict cell death was found to be 13 and 27 W/cm^2 for i-AuNP-treated and dT-AuNP-treated cells (Figure 6b), respectively. This clearly indicates that pH-responsive aggregation of i-AuNP enhances their thermal production. Furthermore, a higher laser power of 44 W/cm^2 failed to inflict cell death on untreated cells (Figure 6b).[34] The absence of dead cells outside the laser spot, regardless of the DNA-AuNP and laser power densities, accentuated the potency of the nanomachine in imparting target specificity and minimal cytotoxicity at low laser power emulating reported Au nanostructures[35−37] in eliciting photothermal ablation.

***In Vitro* Synergistic Effect of Gene Silencing and Photothermal Ablation.** The second facet of the therapeutic application involves the siRNA gene silencing studies established by luciferase gene expression assay in NIH3T3 cells as a model gene silencing system. As described in the earlier sections, the internalization and aggregation of AuNPs were clearly evident from the microscopic and photothermal studies; however, these observations

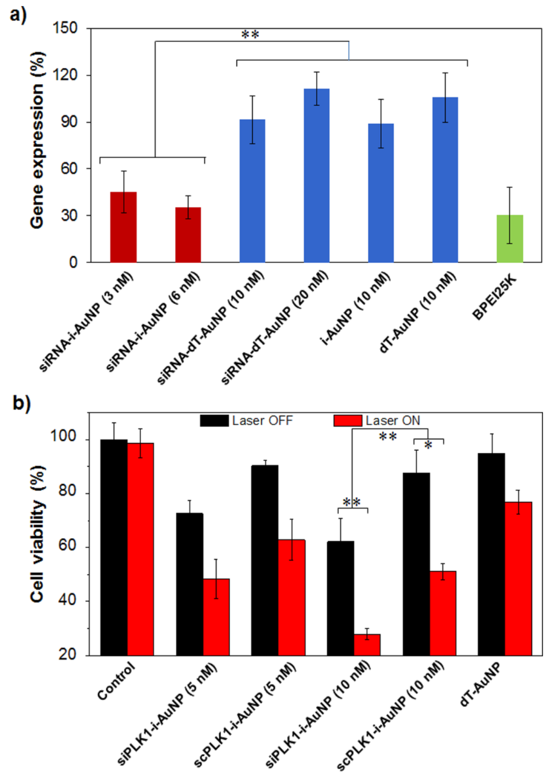

Figure 7. Therapeutic evaluation of DNA nanomachine. (a) DNA nanomachine-mediated gene silencing. Cells were treated with siRNA-i-AuNPs or siRNA-dT-AuNP loading siRNA against luciferase. Control cells were treated with i-AuNP or dT-AuNP without siRNA and BPEI25K/siRNA polyplex (N/P ratio: 10). (b) Synergistic effect of DNA nanomachine in gene silencing and photothermal effect. siRNA against PLK1 was employed. The power of laser irradiation is 2 W/cm^2 (n = 5). The symbol * indicates the statistical significance at levels of $p < 0.05$, and ** indicates $p < 0.01$.

did not shed any light on the programmed release of siRNA strand (Figure 6a) and its efficacy in inducing gene silencing. Therefore, successful gene silencing remained crucial in establishing the potency and fate of the DNA nanomachine as therapeutic device.

The developed model of the therapeutic nanomachine, namely, siRNA-i-AuNPs containing therapeutic siRNA, in comparison to pH-insensitive siRNA-dT-AuNPs and DNA-AuNPs lacking siRNA(i-AuNPs and dT-AuNPs), demonstrated highly efficient gene silencing. Notably, siRNA-i-AuNPs demonstrated a gene silencing efficiency comparable to that of BPEI25K (branched polyethylenimine, M_w 25K) polyplex, the gold standard in polymeric gene silencing, 48 h post-transfection (Figure 7a). Such rapid and efficient gene silencing by siRNA-i-AuNPs in a dose- and intracellular pH-dependent manner can collectively be attributed to several important properties, including resistance of the densely immobilized hybrid DNA-Au nanomachine to nuclease degradation, highly effective pH-response for endosomal escape, and efficient release of siRNA in the cytosol.[38,39]

As mentioned above, the merit of our DNA nanomachine is the ability to accomplish simultaneous gene silencing and photothermal effect for efficient cell death. Therefore, the synergistic effect of DNA nanomachine in gene silencing and photothermal ablation was evaluated. siRNA targeting polo-like kinase 1 (siPLK1) was employed to demonstrate gene silencing effect. PLK1 is an important enzyme in the maintenance of genomic stability and mitosis in cells.[40,41] Thus, the suppression of PLK1 induces apoptosis of cells. The cells were incubated with siPLK1-loaded nanomachine, followed by laser irradiation for photothermal ablation. Then, the synergistic effect of gene silencing and photothermal ablation was estimated by 3-(4,5-dimethylthiazol-2-yl)-2,5-diphenyltetrazolium bromide (MTT) assay (Figure 7b). The cell viability was dramatically decreased in siPLK1-modified AuNPs (siPLK1-i-AuNP) with laser irradiation, which implies that cell death was synergistically accelerated by gene silencing and photothermal ablation. The scrambled scPLK1-i-AuNP showed negligible cell viability compared with siPLK1-i-AuNP, representing the sequence specific gene down-regulation. Therefore, our precisely designed nanomachine was proved as an effective therapeutic agent, maximizing both gene silencing and photothermal effect.

CONCLUSION

In summary, DNA-based Au nanomachine developed in this study demonstrated excellent gene silencing efficacy and highly precise photothermal effect in *in vitro* experiments, and also bears seemingly high potential toward practical therapeutic realization. The ingenious design, successful construction, judicious integration of several favorable traits and effective therapeutic outcome of this hybrid DNA-AuNP nanodevice further advocates the immense possibilities for multimodal exploitation of environmentally responsive devices in regulating biological processes. Successful *in vivo* validation and imparting target specificity could further broaden the scope of therapeutic applications of the nanomachine and may uncover infinite potential for the diverse frontiers of DNA nanotechnology.

EXPERIMENTAL SECTION

Synthesis of Gold Nanoparticles (AuNPs). Citrate-stabilized AuNPs were prepared using well-established procedures.[42] An aqueous solution of hydrogen tetrachloroaurate hydrate (100 mL, 0.05 mM, 99.999%) in ultra pure water was boiled at 120 °C for 20 min, followed by addition of sodium citrate tribasic dehydrate solution (1.5 mL, 1.5 mM). The mixture was boiled for 10 min. The color of solution gradually changed from yellow to purple and finally became red within 5 min. The mixture was subsequently cooled for 30 min at room temperature. Then the mixture was concentrated and purified by filtering through Amicon ultra centrifugal filters (M_w cut off: 100 kDa) three times. The size and morphology of AuNPs were determined by transmission electron microscopy (TEM) analysis (Figure S1, Supporting Information). The absorption coefficient value of AuNPs was estimated to be $\sim 2 \times 10^8$ cm^{-1} M^{-1} using the relationship between core size and extinction coefficient for citrate-stabilized AuNPs. It was observed that AuNPs having 15 nm in diameter were well dispersed into discrete particles in the solution (Figure S1, Supporting Information).

Preparation of Nucleic Acid-Modified AuNP. To prevent the degradation of RNA, all buffers and vials were treated with 0.1% diethylpyrocarbonate (DEPC) for 12 h and autoclaved at 121 °C for 20 min. Prior to use, the disulfide functionality at the end of thiolated DNA was deprotected by incubating with DTT at room temperature for 2 h (0.1 M DTT, 10 mM phosphate buffer, pH 7.5) and subsequently purified by using a PD-10 column. AuNPs were then mixed with purified thiolated DNA strands at a molar ratio (AuNP/DNA) of 1:100. The DNA/AuNP solution was allowed to incubate at room temperature for overnight. Then, the concentration of NaCl solution was gradually increased from 0.1 to 0.3 M by adding 1 M NaCl, and incubated for additional 48 h. Finally, the mixture was centrifuged at 13 000 rpm for 1 h and the supernatant containing free DNA was removed. The precipitated DNA-AuNPs were washed with 10 mM phosphate buffer thrice. The size and morphology of AuNPs were determined by TEM analysis. A high surface coverage (99/AuNPs) was achieved by salt aging process[43] followed by purification through repeated centrifugation and washing. To quantify the average number of DNA immobilized on each AuNP, the known amount of AuNPs was incubated at room temperature with 2 mM KCN solution until reddish solution became transparent to confirm complete dissolution of AuNPs. These mixtures were further incubated at room temperature for 10 min with SYBR Green I (1X), which is a well-known DNA intercalating reagent. The fluorescence intensity of the sample solution was measured with excitation at 497 nm and emission at 520 nm by a spectrofluorophotometer (RF-5301PC, SHIMADZU). Calibration curve was obtained by mixing SYBR Green I with free DNA solution ranging from 0.05 to 1.5 μM. The fluorescence intensities of the samples correlate with the amount of DNA in calibration sample solution. The average number of DNA per AuNP for each aliquot was calculated by dividing the concentration of DNA by the concentration of AuNPs. All experiments were repeated three times using fresh samples to obtain reliable standard curve. Then, siRNA-loaded i-motif AuNPs were prepared by mixing siRNA having overhang with i-motif-AuNPs. siRNA is expected to be hybridized with partly complementary i-motif-AuNPs. Quantification of siRNA loaded onto the i-motif-AuNPs was carried out by SYBR Green assay, following same procedure as described above. Overall 34 mol of siRNA was found to be loaded on the surface of each mol of AuNP.

pH- and Sequence-Dependent AuNPs Aggregation. The pH- and sequence-dependent AuNP aggregation experiments were performed with i-AuNPs, dT-AuNPs, and dA-AuNPs (3 nM, 200 μL) in 10 mM phosphate and acetate buffers containing 10 mM $MgCl_2$. The kinetics of pH (ranging from 2.1 to 7.2) and DNA-sequence dependent AuNP aggregation were evaluated by monitoring optical absorbance changes (from 525 to 615 nm) in AuNPs at different time intervals from 0 to 140 min.

***In Vitro* Cell Assays.** Cells were grown on 12 mm glass coverslips for dark-field and confocal imaging, or directly in gelatin-coated 12-well plates for TEM and photothermal study at a density of 3×10^5 cells/well at 37 °C under 5% CO_2. After 1 day, cells were coincubated for predetermined periods with i-AuNPs, dT-AuNPs, or without AuNPs in 10% serum-containing culture media. For dark-field and confocal imaging, coverslips were fixed using 3.5% formaldehyde and mounted on slide glass using an aqueous mounting media with an antifading agent (Vector Laboratories Inc., Burlingame, CA). For photothermal studies, cells were exposed to a 660 nm CW laser light for 5 min at various power densities, and trypan blue staining was used to reveal cell mortality. For TEM imaging, the cells were fixed in 2.5% glutaraldehyde that was prepared in a 0.1% sodium cacodylate buffer. The samples were subsequently postfixed and stained with 1% aqueous osmium tetroxide and then dehydrated by a series of ethanol solutions (30, 50, 70, 80, 90, and 100% for 10 min each; and twice at 100% for 15 min) prior to being resin-embedded. Thin sections containing the cells (done by ultramicrotome, MT-X, RMC, Tucson, AZ) were placed on grids prior to TEM observation (JEM-1011, JEOL, Tokyo, Japan).

Evaluation of Synergistic Effect of DNA-Au Nanomachine in siRNA-Induced Gene Silencing and Photothermal Ablation. For gene silencing assay, NIH3T3 cells were seeded in 24-well plates and transfected with polyplexes of BPEI25K/pDNA (branched polyethylenimine/pCMV-Luc) (N/P ratio of 10) for 3−4 h in serum free culture media. The media was replaced with fresh 10% serum-containing media with siRNA-i-AuNPs (3 nM and 6 nM AuNPs concentration, siRNA/AuNP= 34) directed against luciferase and further incubated for 2 days. For comparison, we transfected the same amount of luciferase siRNA (siLuc) duplex (100 nM) using BPEI25K as a positive control. Luciferase gene expression was evaluated using a microplate spectrofluorometer (VICTOR3 VTM Multilabel Counter, PerkinElmer−Wellesley MA). Quantification of luciferase expression was normalized to control that had not been transfected. For the synergistic effect of siRNA-i-AuNPs in gene silencing and photothermal effect for cell death, NIH3T3 cells were seeded in 96-well plates at a density of 5×10^3 cells/well. After 24 h, the media was changed with the culture media solutions of siRNA-i-AuNPs containing siPLK1 (5′-AGA UCA CCC UCC UUA AAU Att ttg ggg tta ttt ttt-3′, 5′-UAU UUA AGG AGG GUG AUC Utt-3′) or scPLK1 (5′-CUU ACG CUG AGU ACU UCG Att ttg ggg tta ttt ttt-3′, 5′-UCG AAG UAC UCA GCG UAA Gtt-3′), and further incubated for 2 days. Each well was washed twice with DPBS, and the fresh culture media was added, followed by laser ablation (808 nm CW laser, beam spot size: 1 mm) for 5 min at 2 W/cm^2, and further incubated 24 h at 37 °C under 5% CO_2 humidified condition. After incubation, MTT solution was treated and incubated for 4 h. Then dimethyl sulfoxide (DMSO) was added, and the absorption of 570 nm was measured using a microplate spectrofluorometer (VICTOR3 VTM Multilabel Counter, PerkinElmer-Wellesley MA). The results are presented as the mean and standard deviation of the mean obtained from three samples.

Conflict of Interest: The authors declare no competing financial interest.

Acknowledgment. This work was supported by the Research Center Program of IBS (Institute for Basic Science) in Korea (CA1203-02).

Supporting Information Available: Detail materials and reagents; TEM images of nanoparticles; Confirmation of DNA hybridization; $MgCl_2$ effect on AuNPs aggregates formation; pH- and sequence-dependent AuNPs aggregation; pH-dependent aggregation of AuNPs modified with polydA; Rational design of linker DNA sequence; Confocal microscopy study. This material is available free of charge *via* the Internet at http://pubs.acs.org.

REFERENCES AND NOTES

1. Boyer, P. D. Molecular Motors: What Makes ATP Synthase Spin?. *Nature* **1999**, *402*, 247–249.
2. Hess, H.; Vogel, V. Molecular Shuttles Based on Motor Proteins: Active Transport in Synthetic Environments. *Rev. Mol. Biotechnol.* **2001**, *82*, 67–85.
3. Browne, W. R.; Feringa, B. L. Making Molecular Machines Work. *Nat. Nanotechnol.* **2006**, *1*, 25–35.
4. Kim, W. J.; Sato, Y.; Akaike, T.; Maruyama, A. Cationic Comb-Type Copolymers for DNA Analysis. *Nat. Mater.* **2003**, *2*, 815–820.
5. Ochs, M.; Carregal-Romero, S.; Rejman, J.; Braeckmans, K.; De Smedt, S. C.; Parak, W. J. Light-Addressable Capsules as Caged Compound Matrix for Controlled Triggering of Cytosolic Reactions. *Angew. Chem., Int. Ed.* **2013**, *52*, 695–699.
6. Aathimanikandan, S. V.; Savariar, E. N.; Thayumanavan, S. Temperature-Sensitive Dendritic Micelles. *J. Am. Chem. Soc.* **2005**, *127*, 14922–14929.
7. Hoare, T.; Santamaria, J.; Goya, G. F.; Irusta, S.; Lin, D.; Lau, S.; Padera, R.; Langer, R.; Kohane, D. S. A Magnetically Triggered Composite Membrane for On-Demand Drug Delivery. *Nano Lett.* **2009**, *9*, 3651–3657.
8. Seeman, N. C. DNA in a Material World. *Nature* **2003**, *421*, 427–431.
9. Seeman, N. C. From Genes to Machines: DNA Nanomechanical Devices. *Trends Biochem. Sci.* **2005**, *30*, 119–125.
10. Liu, H.; Liu, D. DNA Nanomachines and Their Functional Evolution. *Chem. Commun.* **2009**, *21*, 2625–2636.
11. Liedl, T.; Sobey, T. L.; Simmel, F. C. DNA-Based Nanodevices. *Nanotoday* **2007**, *2*, 36–41.
12. Choi, S. W.; Makita, N.; Inoue, S.; Lesoil, C.; Yamayoshi, A.; Kano, A.; Akaike, T.; Maruyama, A. Cationic Comb-Type Copolymers for Boosting DNA-Fueled Nanomachines. *Nano Lett.* **2007**, *7*, 172–178.
13. Chen, C.; Pu, F.; Huang, Z.; Liu, Z.; Ren, J.; Qu, X. Stimuli-Responsive Controlled-Release System Using Quadruplex DNA-Capped Silica Nanocontainers. *Nucleic Acids Res.* **2011**, *39*, 1638–1644.
14. Xu, C.; Zhao, C.; Ren, J.; Qu, X. pH-Controlled Reversible Drug Binding and Release Using a Cytosine-Rich Hairpin DNA. *Chem. Commun.* **2011**, *47*, 8043–8045.
15. Chen, L.; Di, J.; Cao, C.; Zhao, Y.; Ma, Y.; Luo, J.; Wen, Y.; Song, W.; Song, Y.; Jiang, L. A pH-Driven DNA Nanoswitch for Responsive Controlled Release. *Chem. Commun.* **2011**, *47*, 2850–2852.
16. Mao, Y.; Liu, D.; Wang, S.; Luo, S.; Wang, W.; Yang, Y.; Ouyang, Q.; Jiang, L. Alternating-Electric-Field-Enhanced Reversible Switching of DNA Nanocontainers with pH. *Nucleic Acids Res.* **2007**, *35*, e33.
17. Kim, H.; Kim, W. J. Photothermally Controlled Gene Delivery by Reduced Graphene Oxide-Polyethylenimine Nanocomposite. *Small* **2014**, *10*, 117–126.
18. Kim, H.; Lee, D.; Kim, J.; Kim, T.; Kim, W. J. Photothermally Triggered Cytosolic Drug Delivery *via* Endosome Disruption Using a Functionalized Reduced Graphene Oxide. *ACS Nano* **2013**, *7*, 6735–6746.
19. Sharma, J.; Chhabra, R.; Yan, H.; Liu, Y. pH-Driven Conformational Switch of "i-motif" DNA for the Reversible Assembly of Gold Nanoparticles. *Chem. Commun.* **2007**, *5*, 477–479.
20. Seela, F.; Budow, S. pH-Dependent Assembly of DNA−Gold Nanoparticles Based on the i-Motif: A Switchable Device with the Potential of a Nanomachine. *Helv. Chim. Acta* **2006**, *89*, 1978–1985.
21. Lieblein, A. L.; Kramer, M.; Dreuw, A.; Furtig, B.; Schwalbe, H. The Nature of Hydrogen Bonds in Cytidine$\cdots$H$^+\cdots$Cytidine DNA Base Pairs. *Angew. Chem., Int. Ed.* **2012**, *51*, 4067–4070.
22. Gehring, K.; Leroy, J. L.; Guéron, M. A Tetrameric DNA Structure with Protonated Cytosine-Cytosine Base Pairs. *Nature* **1993**, *363*, 561–565.
23. Chakraborty, S.; Sharma, S.; Maiti, P. K.; Krishnan, Y. The Poly dA Helix: a New Structural Motif for High Performance DNA-Based Molecular Switches. *Nucleic Acids Res.* **2009**, *37*, 2810–2817.
24. Hill, H. D.; Hurst, S. J.; Mirkin, C. A. Curvature-Induced Base Pair "Slipping" Effects in DNA-Nanoparticle Hybridization. *Nano Lett.* **2009**, *9*, 317–321.
25. Giljohann, D. A.; Seferos, D. S.; Daniel, W. L.; Massich, M. D.; Patel, P. C.; Mirkin, C. A. Gold Nanoparticles for Biology and Medicine. *Angew. Chem., Int. Ed.* **2010**, *49*, 3280–3294.
26. Patel, P. C.; Giljohann, D. A.; Daniel, W. L.; Zheng, D.; Prigodich, A. E.; Mirkin, C. A. Scavenger Receptors Mediate Cellular Uptake of Polyvalent Oligonucleotide-Functionalized Gold Nanoparticles. *Bioconjugate Chem.* **2010**, *21*, 2250–2256.
27. Giljohann, D. A.; Seferos, D. S.; Patel, P. C.; Millstone, J. E.; Rosi, N. L.; Mirkin, C. A. Oligonucleotide Loading Determines Cellular Uptake of DNA-Modified Gold Nanoparticles. *Nano Lett.* **2007**, *7*, 3818–3821.
28. Sönnichsen, C.; Reinhard, B. M.; Liphardt, J.; Alivisatos, A. P. A Molecular Ruler Based on Plasmon Coupling of Single Gold and Silver Nanoparticles. *Nat. Biotechnol.* **2005**, *23*, 741–745.

29. Wang, S. H.; Lee, C. W.; Chiou, A.; Wei, P. K. Size-Dependent Endocytosis of Gold Nanoparticles Studied by Three-Dimensional Mapping of Plasmonic Scattering Images. *J. Nanobiotechnol.* **2010**, *8*, 33.
30. Chithrani, B. D.; Chan, W. C. W. Elucidating the Mechanism of Cellular Uptake and Removal of Protein-Coated Gold Nanoparticles of Different Sizes and Shapes. *Nano Lett.* **2007**, *7*, 1542–1550.
31. Hu, L.; Mao, Z.; Zhang, Y.; Gao, C. Influences of Size of Silica Particles on the Cellular Endocytosis, Exocytosis and Cell Activity of HepG2 Cells. *J. Nanosci. Lett.* **2011**, *1*, 1–16.
32. Lévy, R.; Shaheen, U.; Cesbron, Y.; Sée, V. Gold Nanoparticles Delivery in Mammalian Live Cells: A Critical Review. *Nano Rev.* **2010**, *1*, 4889.
33. Nativo, P.; Prior, I. A.; Brust, M. Uptake and Intracellular Fate of Surface-Modified Gold Nanoparticles. *ACS Nano* **2008**, *2*, 1639–1644.
34. Choi, W. I.; Kim, J.-Y.; Kang, C.; Byeon, C. C.; Kim, Y. H.; Tae, G. Tumor Regression *In Vivo* by Photothermal Therapy Based on Gold-Nanorod-Loaded, Functional Nanocarriers. *ACS Nano* **2011**, *5*, 1995–2003.
35. Huang, X.; El-Sayed, I. H.; Qian, W.; El-Sayed, M. A. Cancer Cell Imaging and Photothermal Therapy in the Near-Infrared Region by Using Gold Nanorods. *J. Am. Chem. Soc.* **2006**, *128*, 2115–2120.
36. Hirsch, L. R.; Stafford, R. J.; Bankson, J. A.; Sershen, S. R.; Rivera, B.; Price, R. E.; Hazle, J. D.; Halas, N. J.; West, J. L. Nanoshell-Mediated Near-Infrared Thermal Therapy of Tumors Under Magnetic Resonance Guidance. *Proc. Natl. Acad. Sci. U. S. A.* **2003**, *100*, 13549–13554.
37. Nam, J.; Won, N.; Jin, H.; Chung, H.; Kim, S. pH-Induced Aggregation of Gold Nanoparticles for Photothermal Cancer Therapy. *J. Am. Chem. Soc.* **2009**, *131*, 13639–13645.
38. Giljohann, D. A.; Seferos, D. S.; Prigodich, A. E.; Patel, P. C.; Mirkin, C. A. Gene Regulation with Polyvalent siRNA–Nanoparticle Conjugates. *J. Am. Chem. Soc.* **2009**, *131*, 2072–2073.
39. Prigodich, A. E.; Alhasan, A. H.; Mirkin, C. A. Selective Enhancement of Nucleases by Polyvalent DNA-Functionalized Gold Nanoparticles. *J. Am. Chem. Soc.* **2011**, *133*, 2120–2123.
40. Liu, X.; Erikson, R. L. Polo-Like Kinase (Plk)1 Depletion Induces Apoptosis in Cancer Cells. *Proc. Natl. Acad. Sci. U. S. A.* **2003**, *100*, 5789–5794.
41. Naito, M.; Ishii, T.; Matsumoto, A.; Miyata, K.; Miyahara, Y.; Kataoka, K. A Phenylboronate-Functionalized Polyion Complex Micelle for ATP-Triggered Release of siRNA. *Angew. Chem., Int. Ed.* **2012**, *51*, 10751–10755.
42. Frens, G. Controlled Nucleation for the Regulation of the Particle Size in Monodisperse Gold Suspensions. *Nat. Phys. Sci.* **1973**, *241*, 20–22.
43. Hurst, S. J.; Lytton-Jean, A. K. R.; Mirkin, C. A. Maximizing DNA Loading on a Range of Gold Nanoparticle Sizes. *Anal. Chem.* **2006**, *78*, 8313–8318.